# CFD Analysis Results on NEXST-1

Shinkyu Jeong and Takashi Misaka
Institute of Fluid Science, Tohoku University, Sendai, Miyagi, 980-8577, JAPAN

**ABSTRACT**

In this study, flow computations were performed on the NEXST-1 (National EXperiment Supersonic Transport) with unstructured mesh solver. Two different meshes and two different turbulence models were used. The computational results were compared with NEXST-1's flight data. As a whole, the computational result showed a good agreement with flight data, except the pressure distribution on the lower surface in $\alpha$_sweep cases.

## Introduction

Japan Aerospace eXploration Agency (JAXA, formerly National Aerospace Laboratory, NAL) started a scaled supersonic experimental aircraft program, called NEXST (National Experimental Supersonic Transport) [1] in 1996 in order to establish advanced design technology, especially based on CFD, for a next generational supersonic civil transport. To prove the developed design technologies, the program included two types of experimental aircraft: un-manned non-powered (NEXST-1) and un-manned jet-powered (NEXST-2). On 10 October 2005 at the Woomera test range, JAXA performed the NEXST-1 flight test successfully. In this study, CFD analysis was conducted on the NEXST-1 to compare the CFD result with the flight test data. The result showed that the result of CFD corresponds to the flight test data except the pressure distribution on lower surface in $\alpha$_sweep cases.

## Flow Solver

In this study, TAS (Tohoku University Aerodynamic Simulation) Codes [2] developed by Nakahashi was used for mesh generation and flow calculation. This code is based on an unstructured mesh system and consists of TAS_MESH and TAS_FLOW. TAS_MESH is a mesh generator with graphical user interface (GUI) tools [3-6]. It generates triangular surface mesh with the advancing front method [3, 4] and tetrahedral volume mesh with Delaunay tetrahedral method [5]. It also generates hybrid volume mesh composed of tetrahedrons, prisms, and pyramids for viscous flows with high Reynolds number [6]. In TAS_FLOW, Navier-Stokes equations are solved on the unstructured mesh by using a cell-vertex finite volume method. HLLEW (Harten-Lax-van Leer-Einfeldt-Wada) method [7] is used for the numerical flux calculations. Second-order spatial accuracy is realized by a linear reconstruction of the primitive variables.

LU-SGS (Lower/Upper Symmetric Gauss-Seidel) implicit method [8] is used for time integration.

In this study, two turbulence models, Spalart-Allmaras (SA) one-equation model [9] and Menter's shear stress transport two-equation model (SST) [10] have been adopted.

SA model adopted here doesn't include the trip term for transition and *ft2* function which intends to suppress production of eddy viscosity due to numerical error. The production of eddy viscosity starts with the free stream value. A variation of the model, SARC, which reduces the eddy viscosity in the regions of high vorticity [11. 12], is also used. In this study, a simple combination using the minimum of the vorticity $\Omega = \sqrt{2\Omega_{ij}\Omega_{ij}}$ and strain rate $\hat{S} = \sqrt{2s_{ij}s_{ij}}$ is used in the modification [12] as follows;

$$S = \Omega + C_{vor} \min(0, \hat{S} - \Omega) \qquad (1)$$

Here, $C_{vor}$ = 1 for the present computations. The modified model computes turbulent vertical flow without adding much dissipation to vortex core.

Menter's SST model uses the k-ω model near wall, and switches to the k-ε model away from the wall. In this study, the following modification is used in the production terms;

$$\tau_{ij}\frac{\partial u_i}{\partial x_j} \cong \mu_t \Omega^2 \qquad (2)$$

## Computational Grids

Hybrid meshes for Navier-Stokes calculation were generated by using TAS_MESH explained in the previous section. Figure 1 show the prism layers near the wall. 35 prism layers were inserted with a minimum space in normal direction of $1\times10^{6}$.

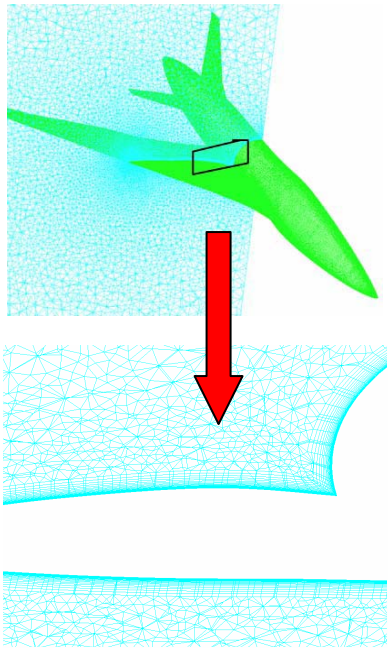

**Figure 1 Computational mesh around the NEXST-1 and the prism layers near the wall**

Two meshes with different density were prepared to investigate the grid dependency. One has 7,575,826 nodes (Grid 1) and the other has 9,990,503 nodes (Grid 2). The surfaces of two meshes are shown in Fig. 2.

## Result and Discussion

Computational conditions are same with the flight test conditions. Mach number, angle of attack, temperature and Reynolds number of the flight test conditions are shown in Tab. 1 and Tab. 2. The conditions in these tables are for pressure and the force measurement, respectively.

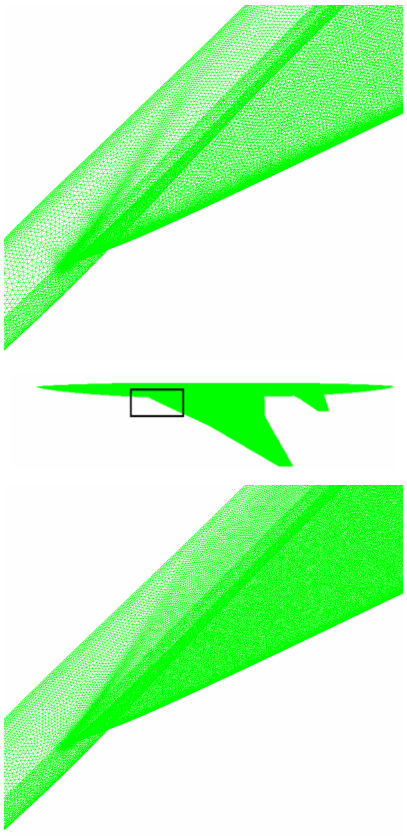

**Figure 2 Surfaces of Grid 1 and Grid 2**

**Table 1 Pressure and transition measurement conditions**

| Case No. | Mach | AOA [deg] | T [K] | Re,unit [1/m] million |
|---|---|---|---|---|
| α_1 | 1.999 | -1.5156 | 372.02 | 4.61 |
| α_2 | 2.016 | -0.0876 | 369.25 | 4.85 |
| α_3 | 2.030 | 0.7666 | 370.83 | 5.17 |
| α_4 | 2.020 | 1.5884 | 372.32 | 5.41 |
| α_5 | 1.998 | 2.5395 | 370.40 | 5.63 |
| α_6 | 1.968 | 3.4519 | 365.14 | 5.74 |
| Re_1 | 1.989 | 1.6952 | 392.64 | 12.34 |
| Re_5 | 1.949 | 1.6834 | 393.90 | 12.72 |
| Re_9 | 1.899 | 1.7079 | 389.78 | 12.59 |

**Table 2 Force measurement conditions**

| Case No. | Mach | AOA [deg] | T [K] | Re,unit [1/m] million |
|---|---|---|---|---|
| α_1 | 2.003 | -1.5571 | 372.58 | 4.60 |
| α_2 | 2.008 | -0.1032 | 369.40 | 4.79 |
| α_3 | 2.031 | 0.7572 | 370.45 | 5.13 |
| α_4 | 2.024 | 1.5943 | 372.30 | 5.39 |
| α_5 | 2.007 | 2.5578 | 370.80 | 5.63 |
| α_6 | 1.989 | 3.4819 | 365.60 | 5.74 |
| Re_1 | 1.989 | 1.7283 | 392.64 | 12.34 |
| Re_5 | 1.949 | 1.7151 | 393.89 | 12.71 |
| Re_9 | 1.903 | 1.6551 | 389.28 | 12.61 |

Grid dependency

To investigate the grid dependency, flow computations were performed with Grid 1 and Grid 2 under the pressure measurement condition of α_4 (M= 2.0206, AOA=1.5884, Unit Re=$5.41\times10^6$) which is the design point of NEXST-1. Spalart-Allmaras model was used as turbulence model with an assumption of full turbulence. Figure 3 shows the pressure distributions at three spanwise sections, 30%, 50%, and 70% for the upper surface and 28%, 48%, and 68% for the lower surface, respectively. However, there is no noticeable different between the result of Grid1 and Grid2. Figure 4 show the CL-AOA and the CL-CD plot. The difference between the result of Grid1 and Grid2 is 0.0005 deg. in $\Delta\alpha_0$, 0.00004 in $\Delta CD_{min}$. Similar to the result of pressure distribution, there is no big difference between the aerodynamic coefficient of Grid1 and Grid 2. Thus, for other computational conditions, only Grid 1 was used.

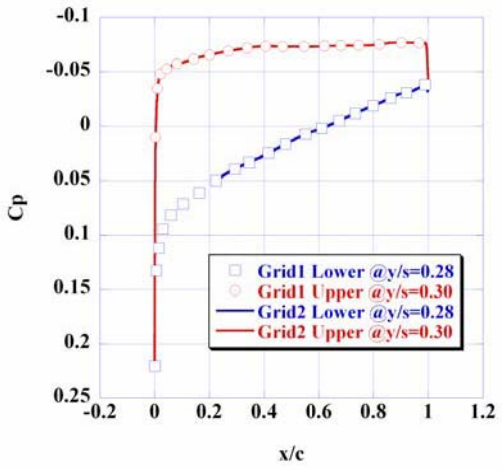


(a) 30% spanwise section

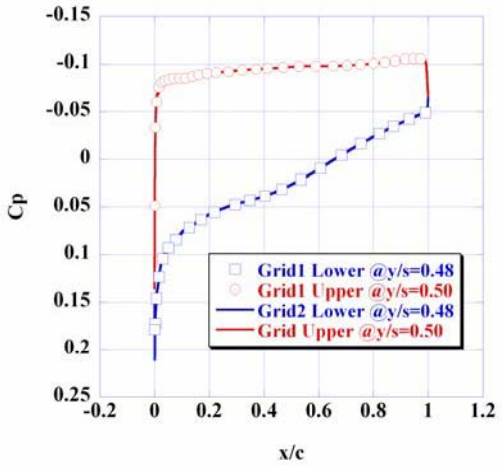


(b) 50% spanwise section

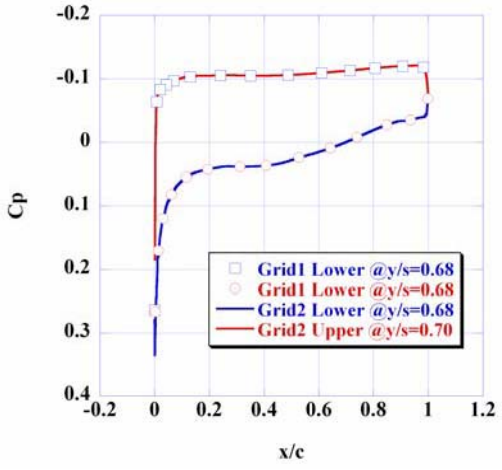


(b) 50% spanwise section

**Figure 3 Pressure distributions**

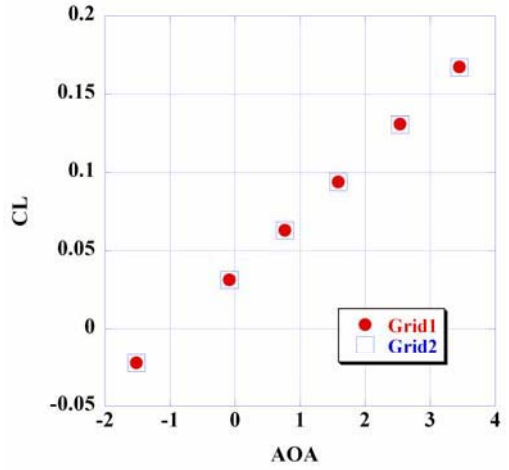


(a) CL-AOA plot

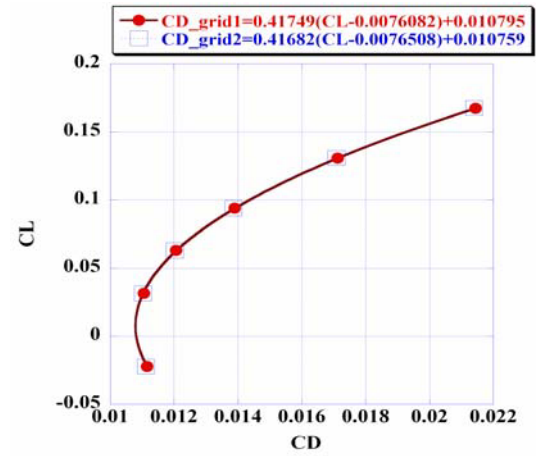


(b) Drag polar

**Figure 4 Aerodynamic coefficients**

Comparison with flight data

Flow computations were performed at the flight test conditions in Table 1 and Table 2. All calculations were done with SA turbulence model under the assumption of full turbulence.

Figure 5 show the pressure distributions of three spanwise sections at the pressure measurement condition, α_4 (M= 2.0206, AOA=1.5884, Unit Re=$5.41\times10^6$). As a whole, the pressure distributions from CFD correspond to the flight test data. However, there exist somewhat large differences on lower surface.

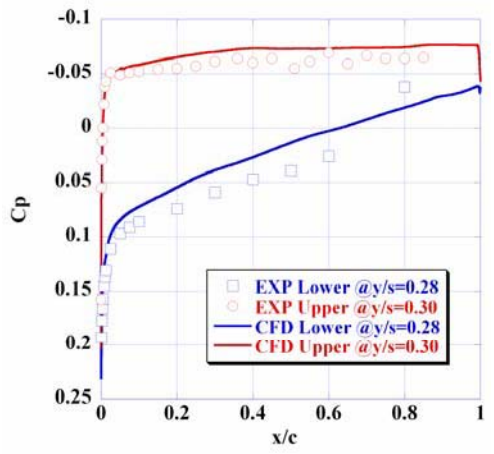


(a) Around 30% spanwise section

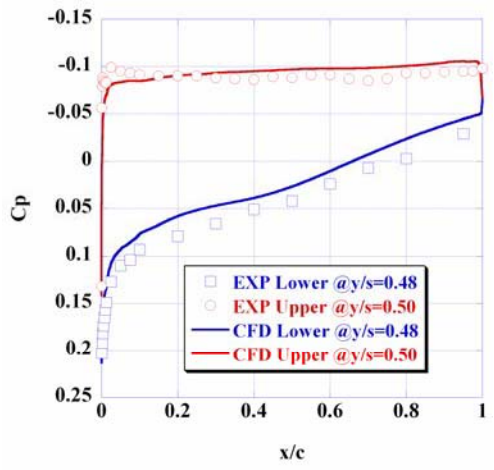


(b) Around 50% spanwise section

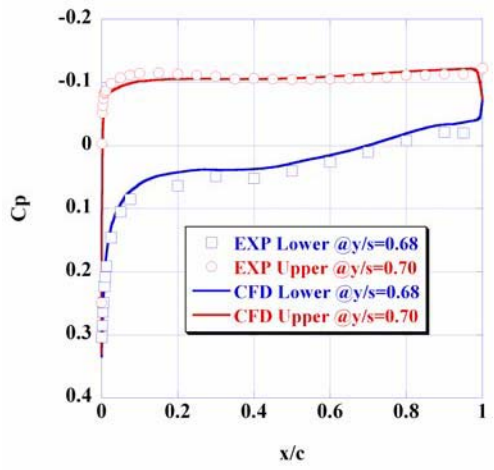


(c) Around 70% spanwise section

**Figure 5 Pressure distributions at the pressure measurement condition, α_4**

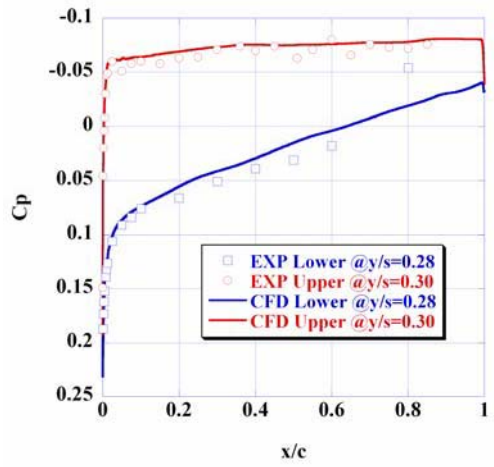


(a) Around 30% spanwise section

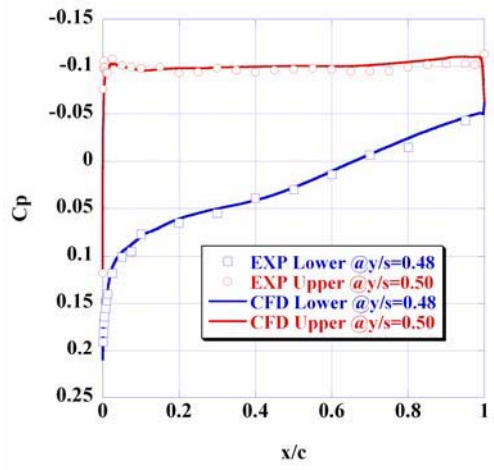


(b) Around 50% spanwise section

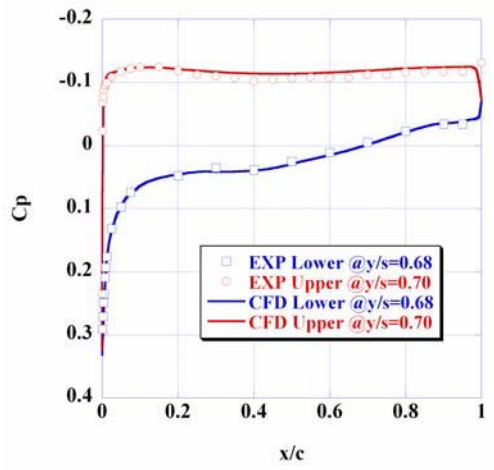


(c) Around 70% spanwise section

**Figure 6 Pressure distributions at the pressure measurement condition, Re_5**

**Table 3 Comparison of CL and CD between SA model and SST model**

| | CL_Total | | | CD_Total | | |
|---|---|---|---|---|---|---|
| | **SA** | **SST** | **SA-SST** | **SA** | **SST** | **SA-SST** |
| **Fuselage** | 0.011087 | 0.01111 | -0.0000250 | 0.003685 | 0.003511 | 0.0001738 |
| **Main Wing** | 0.081989 | 0.08203 | -0.0000390 | 0.009189 | 0.008904 | 0.0002842 |
| **Vertical_W** | 0.000156 | 0.00016 | -0.0000032 | 0.000390 | 0.000359 | 0.0000311 |
| **Horizontal_W** | 0.000805 | 0.00082 | -0.0000119 | 0.000594 | 0.000539 | 0.0000551 |
| **Total** | 0.09403 | 0.094117 | **-0.000079** | 0.013857 | 0.013313 | **0.000544** |

**Table 4 CD decomposed into the pressure and the viscous component**

| | CD_p | | | CD_f | | |
|---|---|---|---|---|---|---|
| | **SA** | **SST** | **SA-SST** | **SA** | **SST** | **SA-SST** |
| **Fuselage** | 0.001273 | 0.001272 | 0.0000011 | 0.002412 | 0.002239 | 0.0001727 |
| **Main Wing** | 0.005627 | 0.005622 | 0.0000045 | 0.003562 | 0.003282 | 0.0002797 |
| **Vertical_W** | 0.000097 | 0.000097 | 0.0000001 | 0.000293 | 0.000262 | 0.0000310 |
| **Horizontal_W** | 0.000217 | 0.000218 | -0.0000004 | 0.000376 | 0.000321 | 0.0000556 |
| **Total** | 0.007214 | 0.007209 | **-0.000005** | 0.006643 | 0.006104 | **0.000539** |

Figure 6 show the pressure distributions at the pressure measurement condition, Re_5 (M= 1.9491, AOA=1.6834, Unit Re=12.72 $\times 10^6$). Differently from α_sweep case, the pressure distributions from CFD coincide with the flight test data not only on upper surface but also on lower surface.

To compare the aerodynamic coefficients, flow computations were conducted at force measurement conditions, α_1 ~α_6. Figure 7 show the CL-AOA and the CL-CD. The difference between the CFD result and the flight test data is 0.3 deg. in $\Delta\alpha_0$ and 0.0005 (5 counts) in $\Delta CD_{min}$.

Effect of turbulence model

To evaluate the effect of turbulence model, flow computation was performed with SST turbulence model at the pressure measurement condition, α_4 (M= 2.0206, AOA=1.5884, Unit Re=5.41×$10^6$). Figure 8 show the pressure distribution of three spanwise sections. However, there was no difference between the result of SA and SST model. In Tab. 3, CL and CD are shown here. While there is no big difference in CL, 5 counts difference exist in CD. For the further investigation, CD was decomposed into the pressure and the viscous component in Tab. 4. The results showed that 5

counts difference between SA and SST model is due to the viscous drag. Generally, SST model has the trend to predict less the shear stress than SA model. This may be the reason of this CD difference between SA and SST model.

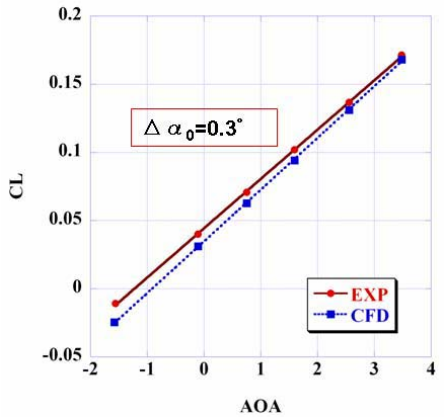


(a) CL-AOA

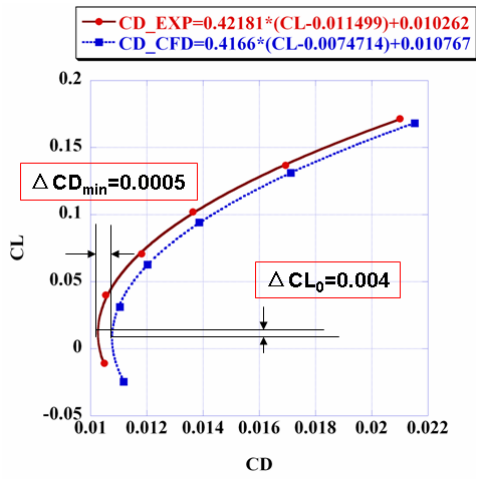


(b) CL-CD

**Figure 7 Aerodynamic coefficients**

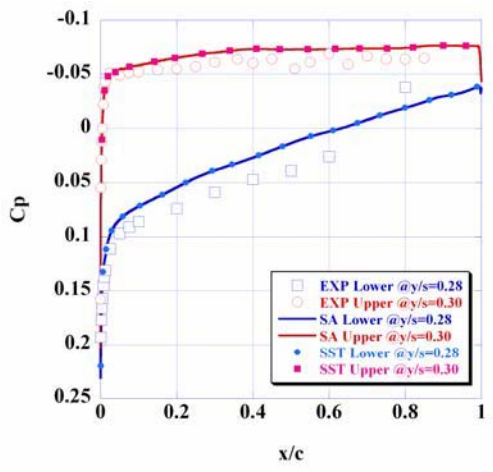


(a) Around 30% spanwise section

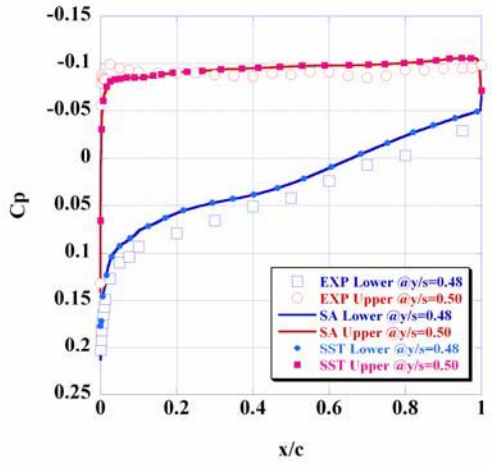


(b) Around 50% spanwise section

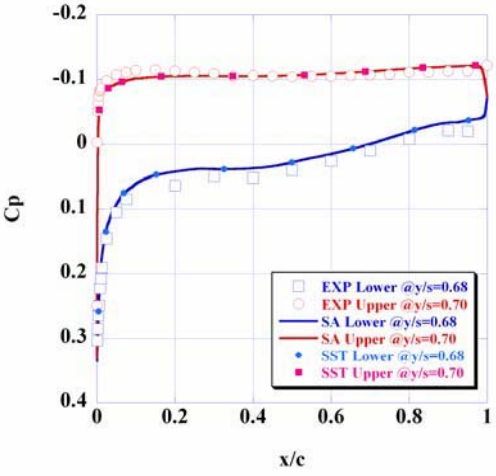


(c) Around 70% spanwise section

**Figure 8 Pressure distributions at the pressure measurement condition, α_4**

## Conclusion

In this study, flow computations were performed on NEXST-1 (National EXperiment Supersonic Transport) configuration to compare with flight test data. TAS (Tohoku University Aerodynamic Simulation) Codes which based on unstructured mesh system was adopted for flow analysis. Grid dependency was investigated by using two grids whose density is different to each other.

CFD result was compared with the flight data. In case of $\alpha$_sweep cases, the pressure distributions of CFD show a good agreement with the flight test data on the upper surface, while there was somewhat large discrepancy on the lower surface. In case of Re_sweep cases, the pressure distributions of CFD coincide with the flight test data both on the upper and the lower surface. From the viewpoint of aerodynamic coefficient, there was 5 counts difference between CFD result and the flight data.

To investigate the effect of turbulence model, flow computation was performed with SA and SST model. There was 5 counts difference between the result of SA model and SST model.

## Reference

[1] Sakata, K., “SST Research Project at NAL”, 1st International CFD Workshop on Supersonic Transport Design, Tokyo, March, 1998.

[2]Nakahashi, K., Togashi, F., Fujita, T., and Ito, Y., “Numerical Simulations on Separation of Scaled Supersonic Experimental Airplane from Rocket Booster at Supersonic Speed,” AIAA Paper 2002-2843, 2002.

[3]Ito, Y. and Nakahashi, K. “Direct Surface Triangulation Using Stereolithography Data,” *AIAA Journal,* Vol. 40, No. 3, pp.490-496, 2002.

[4]Ito, Y. and Nakahashi, K., “Surface Triangulation for Polygonal Models Based on CAD Data,” *International Journal for Numerical Methods in Fluids*, Vol. 39, Issue 1, pp. 75-96, 2002.

[5]Sharov, D. and Nakahashi, K., “A Boundary Recovery Algorithm for Delaunay Tetrahedral Meshing,” Proceedings of 5th International Conference on Numerical Grid Generation in Computational Field Simulations, 1996, pp. 229-238.

[6]Ito, Y. and Nakahashi, K., “Improvements in the Reliability and Quality of Unstructured Hybrid Mesh Generation,”*International Journal for Numerical Methods in Fluids*, Vol. 45, Issue 1, May 2004, pp. 79-108.

[7]Obayashi, S. and Guruswamy, G. P., “Convergence Acceleration of an Aeroelastic Navier-Stokes Solver,” *AIAA Journal*, Vol. 33, No. 6, pp. 1134-1141, 1995.

[8]Sharov, D. and Nakahashi, K., “Reordering of Hybrid Unstructured Grids for Lower-Upper Symmetric Gauss-Seidel Computations,” *AIAA Journal*, Vol. 36, No. 3, pp. 484-486, 1998.

[9]Spalart, P. R. and Allmaras, S. R., “A One-Equation Turbulence Model for Aerodynamic Flows,” AIAA Paper 92-0439, 1992.

[10]Menter, F. R., “Zonal Two Equation k-ω Turbulence Models for Aerodynamic Flows,” AIAA Paper 93-2906.

[11] Dacles-Mariani, J., Zilliac, G. G., Chow, J. S., and Bradshaw, P., “Numerical/Experimental Study of a Wingtip Vortex in the Near Field,” *AIAA Journal*, Vol. 33, No. 9, 1995, pp. 1561-1568.

[12]Lei, Z., “Effect of RANS Turbulence Models on Computational of Separated Flows over a Wing-Body Configuration,” *Proceedings of WCCM VI in conjuction with APCOM”04*, 2004.